

Supporting Information

Chang and Snyder 10.1073/pnas.0913209107

SI Results

Population Analyses Using Alternative Metrics. We feel strongly that fitting data to an explicit and flexible model is a powerful way to characterize cells and determine their frame of reference (Fig. 3A and Fig. S5). However, because our findings of hand-centered and intermediate neurons conflict with previous conclusions drawn from parietal reach region (PRR), we performed three additional analyses, taken from the previously published studies of reference frames for reaching, that were not based on models (1–4).

First, we correlated activity between a pair of conditions with different starting eye positions (*Eyes Left* and *Eyes Right*) and between a pair of conditions with different starting hand positions (*Hand Left* and *Hand Right*) (2, 3). The pattern of activity of gaze-centered cells would be relatively unaffected by change in hand position and therefore would show high correlation coefficients (little change) between *Hand Left* and *Hand Right* conditions (abscissa of Fig. 3B; a measure of gaze-centeredness). In contrast, gaze-centered cells would be substantially affected by a change in eye position and therefore would show low correlation coefficients between *Eyes Left* and *Eyes Right* conditions (ordinate is a measure of hand-centeredness). Hand-centered cells would show the opposite pattern—low correlations between *Hand Left* and *Hand Right* responses and high correlations between *Eyes Left* and *Eyes Right* responses. Because correlations are scale-invariant, gain field modulation should have minimal effect on these patterns.

Of all 259 cells, 52% showed more positive correlations for gaze-centeredness than hand-centeredness (points below the diagonal in Fig. 3B). The results of this analysis roughly matched our classification results using an explicit model: cells with weights close to 1 (red) tend to have high gaze-centeredness, and cells with weights close to 0 (green) tend to have high hand-centeredness. In particular, 81% of the cells that we classified as gaze centered (Fig. 3A) fell below the diagonal line in Fig. 3B, and 94% of hand-centered cells fell above the diagonal line. However, the cells that we classified as intermediate (blue) or indeterminate (black) were evenly distributed across the plot; they did not lie close to the diagonal line as one might expect. Thus, the correlation metric agrees with the explicit model in identifying the presence of both gaze- and hand-centered neurons in PRR. However, the correlation metric does not clearly identify intermediate or unclassifiable cells. Furthermore, although the metric may be robust to the presence of gain fields, it provides no information about them (in contrast to fitting the data to an explicit model that includes gain-field terms).

Second, we calculated a Euclidean distance metric to quantify the sensitivity of neuronal responses to different target locations with changing eye or hand positions (Eq. S1) (4). This method is conceptually similar to the correlation method, but it uses a simpler metric for comparing responses with a set of targets across two conditions (e.g., *Eyes Left* and *Eyes Right*). Briefly, the Euclidean distance for individual cells was computed using

$$\text{Euclidean distance} = \frac{\sqrt{\sum_{i=1}^T (n - m)^2}}{\sqrt{T}}, \quad [\text{S1}]$$

where T represents the number of target locations, n and m represent neuronal responses for different starting eye positions (in case of computing Euclidean distance for different eye positions) or different starting hand positions (in case of computing the distance for different hand positions). The responses n and m are normalized to a scale of 0–1 by subtracting the minimum

response and then, dividing by the maximum response, resulting in a metric that is 0 if the responses are identical and 1 if they are maximally different (ref. 4 has further details).

Like the correlation analysis, this analysis showed a distribution of eye and hand sensitivity with more sensitivity to changes in eye position than hand position (mean difference of 0.04 on a scale of 0–1; $P < 0.005$; two-tailed t test). Just over one-half of the 259 cells (56%) were more sensitive to changes in eye position (Fig. S6A, points below the diagonal), whereas 44% were more sensitive to changes in hand position (points above the diagonal). This was the reverse of the pattern seen in dorsal premotor cortex (PMd), where 42% and 58% of cells were more sensitive to eye and hand positions, respectively (4). Of the well-fit cells, 65% were more sensitive to changes in eye position, and 35% were more sensitive to changes in hand position, again showing a gaze-centered bias (difference of 0.07; $P < 0.0005$). The results closely matched those of the explicit model with 90% of cells modeled as gaze-centered (red) falling below the diagonal and 94% of the cells modeled as hand-centered (green) falling above the diagonal (Fig. S6A). Intermediate and indeterminate cells tended to fall near the diagonal. Thus, the Euclidean distance method compares well with the explicit model.

Third, we subjected our data to a singular value decomposition (1). We constructed two matrices for each cell: one response matrix based on different target locations for different starting eye positions and the other based on different target locations for different starting hand positions. We then obtained sets of three ordered singular values (σ_i) for unique eye and hand positions. Using the three singular values, we computed a separability index (α) for eye and hand (Eq. S2):

$$\alpha = \frac{\sigma_1^2}{\sum_i^3 \sigma_i^2}. \quad [\text{S2}]$$

To determine whether target and eye position or target and hand position are significantly separable, we performed a permutation test ($P < 0.05$) to obtain 95% confidence intervals for each pair for each cell. A gaze-centered cell would show a higher separability index for target and hand positions than for eye and target positions, and a hand-centered cell would show the opposite. In the population ($n = 259$), 65% of cells showed higher indices for target and hand positions than for target and eye positions (i.e., more gaze-centered than hand-centered), and this bias was itself significant ($P < 0.01$; two-tailed t test) (Fig. S6B). Target and eye positions were inseparable for 42% of cells (259 cells total; analogous to gaze-centered), whereas target and hand positions were inseparable for 18% of cells (analogous to hand-centered; permutation test; $P < 0.05$). Twenty percent of cells showed inseparability for target and eye as well as for target and hand positions (analogous to intermediate), and the remaining 20% of cells were separable for target and eye as well as for target and hand (indeterminate; permutation test). The results were similar to those from our explicit modeling (Fig. 3A): 88% of gaze-centered cells showed higher indices of target and hand position pairs, and 78% of hand-centered cells showed higher target and eye position pairs. Intermediate and indeterminate cells were often but not always close to the diagonal (Fig. S6B).

Overall, these additional metrics support our finding of both gaze- and hand-centered neurons in PRR with a bias to gaze-centered and continuous, rather than bimodal, distribution of properties, which is consistent with the existence of intermediate cells.

An ANOVA has also been used to identify the frame of reference used by particular cells. Briefly, the data are subjected to a two-way analysis with factors of gaze-centered target position, hand-centered target position, eye position, and hand position. We find that many cells show a significant effect by ANOVA but on inspection, show no coherent pattern of responses. In our hands, ANOVA provided inferior results, and we, therefore, did not consider it (see below).

Out-of-Bound Cells and Eye–Hand Distance Gain Field. In contrast to in-bound cells, out-of-bound neurons showed significantly greater mismatch between eye and hand gain fields compared with in-bound neurons (Fig. S3B). The median absolute mismatch for in-bound and out-of-bound cells was 1.2 and 3.1% per degree, respectively ($P < 0.005$; Wilcoxon rank sum test). Consistent with this, in-bound cells were overrepresented in the lower quintile(s) of mismatch, whereas out-of-bound cells were overrepresented in the upper quintile(s) of mismatch (Fig. S3B).

Temporal Stability of Reference Frame. If PRR transforms a target representation from one uniform frame of reference (e.g., gaze-centered) to another uniform frame of reference (e.g., hand-centered), it is reasonable to hypothesize that a reference frame used in an early portion of the delay period might be gaze-centered, whereas a reference frame used in a late portion of the delay period might be hand-centered. To address this, we examined the distribution of reference frames at sequential time intervals throughout the duration of the task (200 ms sliding window at a 50-ms step size). We included cells in this analysis as long as they showed at least 5 sp/s of spike-variance explained at any of the sampled 200-ms time windows. Population median weights across different time intervals remained stable throughout the task (Fig. S9). We also examined changes in the model-derived weight parameter relative to the median weight of our population, 0.72 (Fig. 3A and solid line in Fig. S9). Throughout different time epochs, reference frames did not change relative to the population's median weight (two-tailed t test; $P < 0.05$).

Even in the absence of the population-level temporal evolution, individual cells may still dynamically alter their reference frames over time in a more or less balanced way. To test this, we examined the proportion of cells with significant changes in the weight parameter of the general model (Eq. 1) between a visual interval (from 50 to 250 ms relative to target onset) and pre-movement interval (last 200 ms before movement onset). We found that only 12% of those cells with at least 5 sp/s spike-variance explained in both task epochs (11/89 cells) showed a significant change in weight between the two intervals (bootstrap test; $P < 0.05$).

Therefore, consistent with the previous report by Buneo et al. (5), we did not observe clear evidence that the reference frames in PRR dynamically evolve over time. At best, we saw only small and nonsystematic fluctuations over the course of a trial (Fig. S9). This suggests that PRR neurons seem to use diverse, non-uniform reference frames throughout motor planning.

Additional Analysis. Cells with broad tuning may have a different relationship between reference frames and gain fields compared with more narrowly tuned cells. To examine this, we repeated our main analysis separately for cells with tuning widths either greater or less than 40° . The resulting distributions of weights were not significantly different from each other ($P = 0.31$; Wilcoxon signed rank), with median weights of 0.77 ± 0.12 for broadly tuned cells and 0.65 ± 0.09 for narrowly tuned cells. Similarly, the negative coupling of eye and hand gain fields was present in both populations: $r = -0.60$ and -0.59 for the broadly and narrowly tuned cells, respectively (Spearman's rank correlation).

Another method of selecting the cells to include is to show a significant effect in a multiway ANOVA with factors of target

position relative to eye, target position relative to hand, eye position, and hand position. Fig. S7A shows variance explained (Upper) and spike-variance explained (Lower) as a function of the weight parameter of our model; color coding indicates cells that passed a 5 sp/s spike-variance explained criterion or an ANOVA criterion ($P < 0.001$). Fig. S7B shows similar data using a less strict significance criterion for the ANOVA ($P < 0.05$). These plots show that, even at the $P < 0.001$ level, the ANOVA test would include many cells with very low variance explained or low spike-variance explained. There are two possible interpretations of these results. The interpretation that we prefer is that ANOVA is overly sensitive to changes in firing. Because no systematic model is applied, even a nonsystematic deviation in firing in one or more of the test conditions will be taken as evidence for sensitivity to eye or hand position. Alternatively, one can argue that the positive ANOVA in the presence of low variance or spike-variance explained means that there is a source of variation in the data that our model does not capture. This is true almost by definition but does not address if the variation is systematic in relation to a variable of interest.

Finally, some cells might use a frame of reference that is insensitive to both eye and hand positions (e.g., a head-, body-, or world-centered frame). We tested this by comparing fits to the full model (Eq. 1) and a reduced model in which target angle was computed relative to the (fixed) head and body orientation (Eq. 4). Of cells that fit at least one model with at least 5 sp/s spike-variance explained ($n = 108$), the full model explained the data significantly better in 85% of cells (BIC). Therefore, a frame of reference that is insensitive to eye and hand position (e.g., a head-, body- or world-centered frame of reference) cannot account for the vast majority of cells in PRR.

SI Discussion

Accumulating evidence suggests that intermediate frames of reference are common in both sensory and motor regions of the brain. In the intraparietal sulcus (IPS), it has been suggested that posterior parietal neurons use reference frames that are intermediate between gaze- and head-centered for encoding locations for saccades to auditory or visual targets (3, 6, 7). In particular, Mulette-Gillman et al. (3, 7) recorded from the lateral intraparietal area (LIP) and the medial bank of the IPS located across from LIP, regions distinct from PRR, in an auditory and visual saccade task and found that these neurons use mixed frames of reference for encoding target locations (i.e., reference frames in these neurons ranged from gaze- to head-centered and often showed mixed coding schemes for encoding saccade target locations in space) (3, 7). Cells in the superior and inferior colliculus use neither a purely gaze- nor a purely head-centered frame of reference for encoding the location of auditory targets (8–10). The ventral intraparietal area (VIP) and the dorsal medial superior temporal area (MSTd) cells use reference frames that range from gaze- to head-centered for integrating visual and tactile information (11) and for integrating visual and vestibular information (12), respectively. Early studies in PMd reported the use of a uniform hand-centered frame of reference (13, 14). Two recent studies, however, refute this claim. One study reported complex, mixed reference frames in PMd, with some cells using a hand-centered frame of reference and others using a gaze-centered frame; many (52%) used neither a hand- nor a gaze-centered frame (4). Another study reported that PMd neurons encode relative spatial relationships among eye, hand, and target positions in 1D or 2D (1). Around the time of reach movement onset, responses of V6A neurons cannot be fully explained by a gaze-centered reference frame and an eye position gain field, suggesting that some V6A neurons use a non-retinocentric frame of reference (15).

SI Methods

All procedures conformed to the Guide for the Care and Use of Laboratory Animals and were approved by the Washington University Institutional Animal Care and Use Committee.

General Recording Procedures. Eye position was monitored by the scleral search coil technique (CNC Engineering). Hand position was monitored by a 13.2×13.2 -cm custom-built touch panel that uses finely spaced (3 mm) horizontal and vertical infrared beams 1–3 mm above a smooth-touch surface (2-ms temporal resolution). The touch screen was mounted such that the center was approximately aligned with the line of sight when the eyes were estimated to be in primary position. The screen center then formed the origin of our coordinate system for measuring eye and hand position. All measurements are, therefore, in screen coordinates (i.e., the location at which eyes intercept the screen and the location at which the animal touches the screen). As shorthand, we refer to these measurements throughout the text as eye and hand position, respectively. We define a hand-centered representation of a target position as the location of the target in a coordinate system whose origin coincides with the location of the hand, or equivalently, a vector extending from the location of the hand to the location of the target.

The animals sat in a custom-designed monkey chair (Crist Instrument) with a fully open front to provide unimpaired reaching movements. Visual stimuli were back-projected by a CRT (cathode ray tube) projector onto the touch surface, which was mounted vertically about 25 cm in front of the animal. The recording room was sound-attenuating and lightproof, such that a dark-adapted human could detect no light when the projector was turned on but projecting no targets. Extracellular recordings were made using glass-coated tungsten electrodes (Alpha Omega). We recorded neuronal activity in PRR and identified 259 well-isolated, stable cells that showed spatial tuning. Cells were recorded from the right hemisphere from monkey G ($n = 102$) and left hemisphere from monkey S ($n = 157$), with each animal reaching using its contralateral limb. To guide the placement of our recording tracks and localize recording sites, we acquired high-resolution MRI of the monkeys' brains with an MR lucent "phantom" in the recording chamber using methods described elsewhere (16–18). We then created custom MRI atlases for each animal and used those atlases to aim electrodes at the posterior end of the medial bank of the IPS. Based on the MRI-mediated maps, electrodes were lowered, aiming at locations along the medial bank of IPS (~90% of tracks). Localization was accurate to within 1 mm, as determined by injecting and then visualizing MR-lucent manganese in the brain in several sessions.

Behavioral Tasks. The number of targets, spacing, and eccentricity were established using a series of simulations. We simulated neuronal responses to a variety of task designs using idealized cells whose characteristics (tuning width, response variability, etc.) were based on cells that we recorded from PRR in previous studies (16, 17, 19). We varied the task parameters, used our idealized cells to generate artificial data, and then, analyzed those data to optimize the task design and ensure that the fitting procedure was reliable.

We recorded neurons from two monkeys (*Macaca mulatta*) during a visually guided delayed reaching task. These data were also used for a previous report (20). We first mapped each neuron's preferred direction (Fig. S1B). Obtaining a full tuning curve, including the peak neuronal response, is critical for distinguishing reference frame effects from gain field effects (7). For our main task (Fig. 1B), we centered an array of five targets on each cell's preferred direction.

In the preferred direction mapping task, animals made center-out arm movements while maintaining central fixation (19). Animals first fixated and pointed at a blue center target ($2.4^\circ \times 2.4^\circ$ within a 4° radius). A peripheral target ($2.4^\circ \times 2.4^\circ$) ap-

peared at 1 of 16 locations at $12\text{--}14^\circ$ eccentricity. After a variable delay (800–1,200 ms), the center target shrank to a single pixel ($0.3^\circ \times 0.3^\circ$), signaling the animal to reach to the peripheral target without breaking eye fixation. The preferred direction (i.e., the direction associated with the peak neuronal response) (Fig. S1B) determined the target placement for the main task. Capturing the peak response is critical for distinguishing reference frame effects from gain field effects (7). Our method worked well: 91% of the cells with at least 5 sp/s of spike-variance explained showed peak firing at one of three central target locations ($T2\text{--}T4$).

In the main task (Fig. 1B), an initial eye target and an initial hand target, each $0.9^\circ \times 0.9^\circ$, were each presented at one of three possible locations ($P1\text{--}P3$). Monkeys fixated the initial eye target and touched the initial hand target. One or both of the two initial targets were always at the center of the screen, directly in front of the animal ($P2$). The other two possible targets ($P1$ and $P3$) were located 7.5° to either side of $P2$ along an imaginary line through the center of the screen and perpendicular to the cell's preferred direction, as determined in the preferred direction mapping task. Five different configurations of the starting eye and hand position were used (see box in Fig. 1B). Four hundred and fifty ms after the animal touched and fixated the initial hand and eye targets, a peripheral target for a final reach ($2.4^\circ \times 2.4^\circ$) appeared at one of eight possible target locations. These peripheral targets lay in or near the receptive field ($T1\text{--}T5$ in Fig. 1B; spaced 7.5° apart), lying on a line perpendicular to the preferred direction and $12\text{--}14^\circ$ away from the center target ($P2$ to $T3$). There was also one target opposite to the preferred direction and two targets orthogonal to the preferred direction, but data from these targets were not analyzed ($T6$, $T7$, and $T8$). On each trial, animals maintained the initial eye and hand position within 4° and 5° , respectively, for a variable delay period (900–1,300 ms) after the peripheral target onset. The initial eye and hand targets then shrank to a single pixel, cueing the animal to reach out and touch within $5\text{--}6^\circ$ of the peripheral target without moving the eyes from the initial eye target. A median and mode of 8 ± 1.11 repetitions (\pm SD) were collected for each of the 40 unique trial types from each cell in the main task (Fig. 1B). When an error occurred (a failure to achieve or maintain fixation or touch at the initial targets throughout the delay period, inaccurate reach to the peripheral target, or failure to maintain fixation during the reach), the trial was aborted, a multicolored square appeared briefly on the screen as a familiar error signal, and a short (0.5–1.5 s) timeout ensued. Aborted trials were excluded from further analyses. Successful trials were rewarded with a drop of water or juice. Results and Table S1 show reaction times and success rates of individual monkeys.

Details on Model Parameters. The full model (Eq. 1) inputs were firing rates, target eccentricity along the preferred direction (*ecc*; the distance between $P2$ and $T3$ in Fig. 1B measured in degrees of visual angle), target displacement in a direction perpendicular to the preferred direction (*T*; degrees of visual angle measured along the line connecting $T1$ to $T5$), and displacement of the initial eye (*E*) and hand target (*H*) from the center point ($P2$) in degrees of visual angle. We use the terms gaze or eye position and hand position to define the location on the screen at which we measured eye and hand positions (i.e., fixation and pointing positions in 2D screen coordinates). The output parameters were baseline (*k*) and peak amplitude of modulation (*pa*), both in spikes per second, offset of the center of the tuning curve from the central target ($T3$) in degrees of visual angle (*mid*), standard deviation (*sd*) of the Gaussian curve in degrees of visual angle, the amplitudes of the eye-position gain field (g_{Eye}) and the hand-position gain field (g_{Hand}), both in fractional modulation per degree, and a unitless weight parameter (*weight*). The *weight* parameter described the frame of reference for each cell with

weights of 1 and 0 corresponding to pure gaze- and hand-centered cells, respectively. During the fitting procedure, parameters were constrained as follows: from -5 to 100 sp/s for k , from 0 to 300 sp/s for pa , from -1.5 to 2.5 for $weight$, from -0.15 to 0.15 (-15% to 15%) of modulation per degree for g_{Eye} , g_{Hand} , and g_{Diff} , from -45 to 45° for mid , and from 15 to 60° for sd . These constraints were based on previously recorded data and inspection of model fits.

Location of PRR. PRR cells straddle the boundary between the medial intraparietal area (MIP) and V6A in posterior parietal cortex (PPC). PRR was first identified as a region with a high proportion of neurons with strong visual responses and memory activity for visually presented targets that is much stronger on

impending reach trials than on impending saccade trials (19). This region lies on the posterior portion of the medial bank of the IPS, close to the junction with the parieto-occipital sulcus (POS), and may extend onto the lateral bank (Fig. 1D and Fig. S14) (16, 17, 19). By combining our functional definition of PRR with published histological tract tracing data, it can be seen that PRR primarily overlaps the anterior portion of V6A, the posterior portion of MIP, and a small part of LOP/cIPS (Fig. 1D and Fig. S14). Although the borders of these anatomically defined areas vary somewhat from animal to animal and can vary greatly from study to study (21), it is clear that PRR is well separated from LIP and from the portion of the medial bank that lies directly across from LIP.

1. Pesaran B, Nelson MJ, Andersen RA (2006) Dorsal premotor neurons encode the relative position of the hand, eye, and goal during reach planning. *Neuron* 51:125–134.
2. Batista AP, Buneo CA, Snyder LH, Andersen RA (1999) Reach plans in eye-centered coordinates. *Science* 285:257–260.
3. Mullette-Gillman OA, Cohen YE, Groh JM (2005) Eye-centered, head-centered, and complex coding of visual and auditory targets in the intraparietal sulcus. *J Neurophysiol* 94:2331–2352.
4. Batista AP, et al. (2007) Reference frames for reach planning in macaque dorsal premotor cortex. *J Neurophysiol* 98:966–983.
5. Buneo CA, Batista AP, Jarvis MR, Andersen RA (2008) Time-invariant reference frames for parietal reach activity. *Exp Brain Res* 188:77–89.
6. Striccanne B, Andersen RA, Mazzoni P (1996) Eye-centered, head-centered, and intermediate coding of remembered sound locations in area LIP. *J Neurophysiol* 76:2071–2076.
7. Mullette-Gillman OA, Cohen YE, Groh JM (2009) Motor-related signals in the intraparietal cortex encode locations in a hybrid, rather than eye-centered reference frame. *Cereb Cortex* 19:1761–1775.
8. Jay MF, Sparks DL (1984) Auditory receptive fields in primate superior colliculus shift with changes in eye position. *Nature* 309:345–347.
9. Jay MF, Sparks DL (1987) Sensorimotor integration in the primate superior colliculus. II. Coordinates of auditory signals. *J Neurophysiol* 57:35–55.
10. Metzger RR, Mullette-Gillman OA, Underhill AM, Cohen YE, Groh JM (2004) Auditory saccades from different eye positions in the monkey: Implications for coordinate transformations. *J Neurophysiol* 92:2622–2627.
11. Avillac M, Denève S, Olivier E, Pouget A, Duhamel JR (2005) Reference frames for representing visual and tactile locations in parietal cortex. *Nat Neurosci* 8:941–949.
12. Fetsch CR, Wang S, Gu Y, Deangelis GC, Angelaki DE (2007) Spatial reference frames of visual, vestibular, and multimodal heading signals in the dorsal subdivision of the medial superior temporal area. *J Neurosci* 27:700–712.
13. Caminiti R, Johnson PB, Galli C, Ferraina S, Burnod Y (1991) Making arm movements within different parts of space: The premotor and motor cortical representation of a coordinate system for reaching to visual targets. *J Neurosci* 11:1182–1197.
14. Kalaska JF, Scott SH, Cisek P, Sergio LE (1997) Cortical control of reaching movements. *Curr Opin Neurobiol* 7:849–859.
15. Marzocchi N, Breveglieri R, Galletti C, Fattori P (2008) Reaching activity in parietal area V6A of macaque: Eye influence on arm activity or retinocentric coding of reaching movements? *Eur J Neurosci* 27:775–789.
16. Calton JL, Dickinson AR, Snyder LH (2002) Non-spatial, motor-specific activation in posterior parietal cortex. *Nat Neurosci* 5:580–588.
17. Chang SW, Dickinson AR, Snyder LH (2008) Limb-specific representation for reaching in the posterior parietal cortex. *J Neurosci* 28:6128–6140.
18. Kalwani RM, Bloy L, Elliott MA, Gold JI (2009) A method for localizing microelectrode trajectories in the macaque brain using MRI. *J Neurosci Methods* 176:104–111.
19. Snyder LH, Batista AP, Andersen RA (1997) Coding of intention in the posterior parietal cortex. *Nature* 386:167–170.
20. Chang SW, Papadimitriou C, Snyder LH (2009) Using a compound gain field to compute a reach plan. *Neuron* 64:744–755.
21. Lewis JW, Van Essen DC (2000) Mapping of architectonic subdivisions in the macaque monkey, with emphasis on parieto-occipital cortex. *J Comp Neurol* 428:79–111.

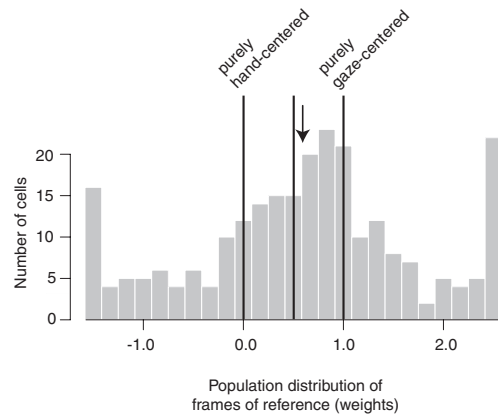


Fig. 55. The distribution of reference frame weights from the delay period is shown for all cells that converged to the full model (Eq. 1) ($n = 255$ of 259 cells). The three vertical lines represent values corresponding to a pure hand-centered representation (weight = 0), a pure gaze-centered representation (weight = 1), and a representation halfway in between the two (weight = 0.5). The arrow indicates the median of the distribution.

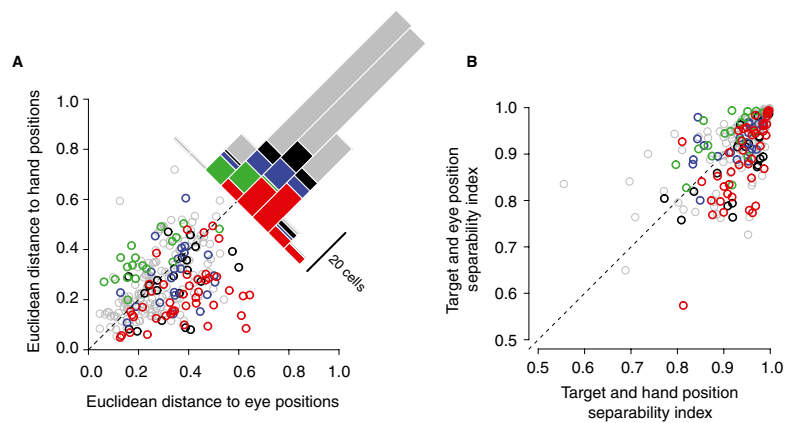


Fig. 56. Additional reference frame analyses. Data from all 259 cells are shown in each panel. Cells with a spike-variance explained of at least 5 sp/s are shown in color: red for gaze-centered cells, green for hand-centered cells, blue for intermediate cells, and black for indeterminate cells based on stepwise regression. Cells with spike-variance explained of less than 5 sp/s are gray. (A) Tuning shift analysis based on the Euclidean distance method. Euclidean distances for different starting eye positions and hand positions are plotted. (B) Tuning shift analysis using the singular value decomposition method. The separability indices are plotted for target and eye positions against target and hand positions.

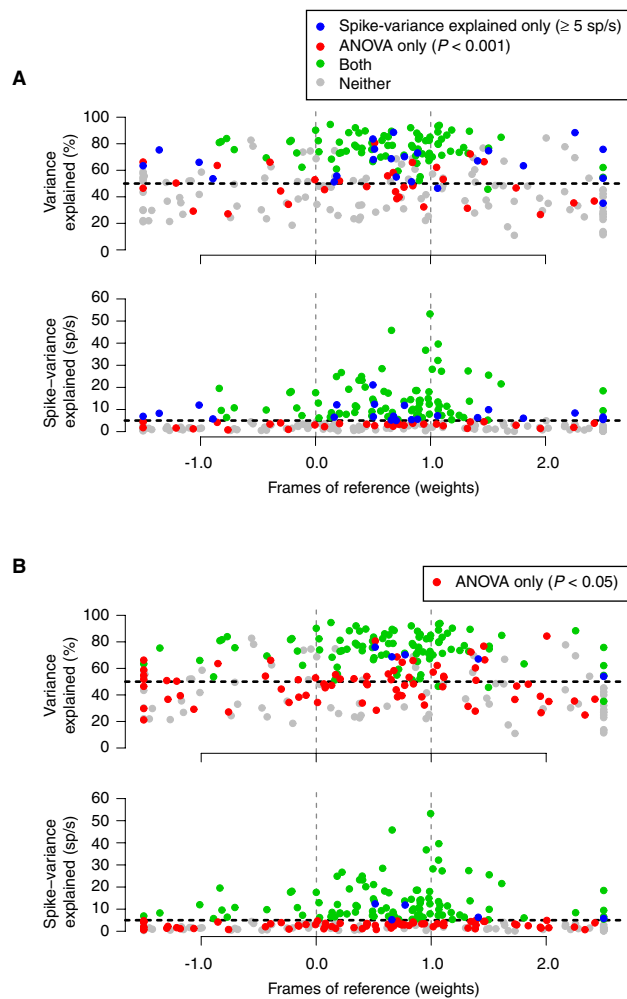


Fig. 57. Comparison of variance explained, spike-variance explained, and ANOVA. (A) Variance explained (r^2) and spike-variance explained are plotted as a function of reference frame (weight parameter from Eq. 1). Color coding indicates selection by ANOVA ($P < 0.001$; red), spike-variance explained (a stepwise regression performed on the full model; Eq. 1; blue), or both (green). The dotted horizontal lines in *Upper* and *Lower* indicate a variance explained of 50% and spike-variance explained of 5 sp/s, respectively. (B) Similar plots comparing cells selected but using a less strict ANOVA criterion ($P < 0.05$). Same format as in A.

